A Method for Charging Electric Vehicles with Battery-supercapacitor Hybrid Energy Storage Systems to Improve Voltage Quality and Battery Lifetime in Islanded Building-level DC Microgrids

Seyyed Ali Ghorashi Khalil Abadi, *Student Member, IEEE,* Jeewon Choi, *Student Member*, *IEEE*, and Ali Bidram, *Senior Member, IEEE*

***Abstract*—This paper proposes a methodology to increase the lifetime of the central battery energy storage system (CBESS) in an islanded building-level DC microgrid (MG) and enhance the voltage quality of the system by employing the supercapacitor (SC) of electric vehicles (EVs) that utilize battery-SC hybrid energy storage systems. To this end, an adaptive filtration-based (FB) current-sharing strategy is proposed in the voltage feedback control loop of the MG that smooths the CBESS current to increase its lifetime by allocating a portion of the high-frequency current variations to the EV charger. The bandwidth of this filter is adjusted using a data-driven algorithm to guarantee that only the EV's SC absorbs the high-frequency current variations, thereby enabling the EV's battery energy storage system (BESS) to follow its standard constant current-constant voltage (CC-CV) charging profile. Therefore, the EV's SC can coordinate with the CBESS without impacting the charging profile of the EV's BESS. Also, a small-signal stability analysis is provided indicating that the proposed approach improves the marginal voltage stability of the DC MG leading to better transient response and higher voltage quality. Finally, the performance of the proposed EV charging is validated using MATLAB/Simulink and hardware-in-the-loop (HIL) testing.**

***Index Terms*—Adaptive filters, constant power loads, electric vehicles, energy storage systems, supercapacitor, transient voltage stability.**

NOMENCLATURE

A. Abbreviations

ARX	Autoregressive with extra input
BESS	Battery energy storage system
BIC	Bidirectional interlinking converter
CBESS	Central battery energy storage system
CC-CV	Constant current-constant voltage
CPL	Constant power load
DER	Distributed energy resource
EMS	Energy management system
ESS	Energy storage system
EV	Electric vehicle
FB	Filtration-based
HESS	Hybrid energy storage system
HIL	Hardware-in-the-loop
HPF	High pass filter
LPF	Lowe pass filter
LTI	Linear time invariant
MG	Microgrid
PI	Proportional-integral
PV	Photovoltaic
RES	Renewable energy source
RLS	Recursive least square
SAPV	Sum of absolute power variations
SC	Supercapacitor
SoC	State of charge

B. Parameters

C_{bus}	MG's DC bus total capacitance
d_1	Duty cycle of the CBESS boost converter
d_2	Duty cycle of the EV charger boost converter
i_{EV}	Output current of the EV
i_{EV}^{SC}	Output current of the EV's SC
i_{HESS}	Output current of the EV's HESS
i_{ref}	Reference current taken from the voltage controller
i_{L1}	Inductor currents of the CBESS converter
i_{L2}	Inductor currents of the EV charger converter
i_{st}^{EV}	Standard charging current of the EV's BESS
K_f	Filtering constant
K_{P1}, K_{I1}	Proportional and integral gains of the CBESS PI current controller
K_{P2}, K_{I2}	Proportional and Integral gains of the EV charger PI current controller
K_{Pv}, K_{Iv}	Proportional and Integral gains of the MG PI voltage controller
L_1	Inductance of the CBESS converter filter
L_2	Inductance of the EV charger converter filter

Manuscript received October 30, 2022; revised February 3, 2023; accepted March 6, 2023. This material is based upon work supported by the National Science Foundation under Awards OIA-1757207 and ECCS-2214441. *(Corresponding author: Seyyed Ali Ghorashi Khalil Abadi)*

The authors are with the Department of Electrical and Computer Engineering, University of New Mexico, MSC011100, 1 University of New Mexico, Albuquerque, USA. (e-mail: ghorashi@unm.edu chatchi923@unm.edu; bidram@unm.edu).

P_{CBESS}	Output power of the CBESS
P_{CPL}	CPL power demand
P_{EV}	Output power of the EV
P_{EV}^{SC}	Output power of the EV's SC
P_{HESS}	Output power of the EV's HESS
P_{PV}	PV power generation
R_1	Resistance of the CBESS converter filter
R_2	Resistance of the EV charger converter filter
T_s	Sampling time
v_{bus}	MG DC bus voltage
$\hat{v}_{bus}$	Measured DC bus voltage
v_{bus}^*	Nominal or reference DC bus voltage
v_{EV}	Terminal voltage of the EV' HESS
x_d	State of Pade approximation of the delay
x_f	State of the current allocation filter
$x_{\text{int}1}$	State of the CBESS current controller
$x_{\text{int}2}$	State of the EV charger current controller
$x_{\text{int}v}$	State of the MG voltage controller
τ_c	Time constant of the CBESS power smoothing filter
τ_d	Time delay of the voltage measurements
ω_c	Cut off frequency of the CBESS power filter
ω_H	Cut off frequency of the EV power filter
ω_H^*	Estimated cut off frequency of the EV filter

I. INTRODUCTION

Microgrids are autonomous distributed energy systems that can promote the reliability, resiliency and flexibility of traditional power systems [1]. Recently, DC MGs have drawn remarkable attention due to their fewer power conversion losses and lower control complexity compared to AC MGs [2]. Besides, DC MGs can be easily adopted to integrate RESs (e.g., photovoltaic and wind), ESSs, and EVs. Therefore, DC MGs are counted as feasible solutions for grid modernization, and effective integration of RESs as well as supplying remote rural areas in which there is no access to the utility grid.

Latterly, developing the DC MGs for building-level applications (i.e., building-level DC MGs) has gained significant interest in both academia and industry [3]. A Building-level DC MG, also called a DC nano-grid, is an autonomous small-scale low-voltage DC distribution system supplying a residential or commercial building. Building-level DC MGs are typically designed based on single bus configurations and contain a group of local loads, local power generation units (e.g., a CBESS, and PV), and an AC to DC bidirectional interlinking converter (BIC) that enables the power exchange with the upstream AC grid [4]. In this configuration, during the grid-connected mode the MG, the BIC system operates as the slack terminal and maintains voltage stability and power balance of the DC MG while the CBESS is in grid-following mode and operates as a power terminal. Consequently, in grid connected mode of the MG, the output power of the CBESS is not usually affected by the instantaneous variations of the PV power or loads [5].

On the other hand, the building-level DC MGs can operate autonomously to supply their local loads when the upstream grid is not available. In the islanded mode of operation, the CBESS of the MG operates as the grid-forming unit to regulate the DC bus voltage and maintain the balance between power generation and loads. So, the output power/current of the CBESS can be affected by the instantaneous power fluctuations of the loads or PV that results in frequent charging and discharging the CBESS. Hence, during the islanded mode , the rapid variations of renewable power or load can degrade the grid-forming CBESS due to the limited life cycle of batteries [6]. In addition, it can increase the battery's temperature which results in reducing the CBESS lifetime [7].

To expand the lifespan of the BESSs, an SC can be utilized in tandem with the BESSs. This combination forms a battery-supercapacitor HESS [8]. In this technology, due to the almost unlimited life-cycle and noticeably higher power density of SCs, the SC absorbs/releases the high current rates, and the BESS is responsible for long-term energy storage because of its larger energy density [9]. To this end, a low-pass filter is usually applied to perform the power/current assignment between the BESS and SC by decomposing the input power/current of the HESS into low and high-frequency components and allocating the high-frequency parts to SC [10]. For instance, a distributed rule-based power management strategy with an adaptive power smoothing filter was proposed for a residential DC MG that utilizes a PV and a battery-SC HESS unit [11]. In this system, regarding the SoC of the SC, a portion of high-frequency power variations of the PV is absorbed by the SC to smooth out the BESS power profile. Besides, a battery lifetime and life cycle cost analysis for a battery-SC HESS was proposed in [12]. This study shows that a battery-SC HESS that utilizes a rule-based EMS with a power smoothing filter (i.e., the conventional HESS control structure) can 14.8% extend the lifetime of the battery while it is just 5.36% more expensive than a single lead-acid battery in terms of the life cycle cost. Intelligent control of DC MGs with HESSs was also proposed in [13] which improved the overall efficiency and reliability of the system by ensuring the power balance between RESs and HESS units. Also, the design and stability analysis of DC MGs with HESSs was studied in [14]. This study examined the sensitivity of the DC MG stability to the SC terminal voltage and suggested a method to determine the optimal value of SC voltage for enhancing the voltage stability of the DC MGs with HESS technologies. A model predictive control strategy was also suggested for a grid-forming battery-SC HESS unit in a small-scale residential DC MG [15]. It was shown that this method not only increased the lifetime of the BESS but also improved the marginal voltage stability of the system.

In addition to the renewable power fluctuations and CBESS degradation issue, CPLs can create some challenges for the operation of building-level DC MGs. CPLs are typically

electronic loads that utilize a point-of-load converter for power conditioning and voltage control [16]. They demand steady power under varying voltage at the MG side. The main characteristic of CPLs is their negative incremental resistance that tends to destabilize the system [17]. CPLs can create serious voltage stability issues in building-level DC MGs due to the high penetration of electronic loads and point-of-load converters. Consequently, the building-level DC MGs (or DC nano-grids) require large marginal stability of the MG voltage controller [18]. One way to achieve this is to design the PI voltage controller with small gains to guarantee the voltage stability of the MG with nominal values of CPLs [19]. However, the very small gains of the PI voltage controllers may lead to high transient voltage deviations during the load changes. On the other hand, different active compensation techniques can be implemented to improve the marginal stability of the system [20]. However, these techniques may cause steady-state voltage deviations at MG DC bus and their stability improvement is sometimes insufficient [18]. To tackle the stability issues created by CPLs, the conventional PI voltage controllers can be replaced with a variety of advanced control techniques such as nonlinear controllers [21], adaptive controllers [22], or model predictive controllers [23]. However, the design of advanced controllers may add significant complexity to the primary control layer of the DC MG which in turn affects the flexibility and scalability of the system.

Recently, EVs are spreading rapidly around the world because of their low operation and maintenance costs and no pollution emissions. ESS design is one of the major concerns in EV research and development activities that impact the EV price and range [24]. Similar to the MG applications, battery-SC HESS technologies can be utilized in EVs to expand the lifespan of the EVs' BESSs. The HESS may have different topologies in EV applications including passive, semi-active and active topologies among which the semi-active topology with a filtration-based current allocation system supervised by a rule-based EMS is the most popular configuration [25]. An experimental study of semi-active battery-SC HESSs for EV applications was performed in [26]. This study revealed that a semi-active HESS that incorporates a filtration-based current sharing system supervised by a fuzzy rule-based EMS can reduce the capacity fade cost of the battery up to almost 50% compared to the conventional standalone BESS configurations.

Bidirectional power flow between EVs and the MG, namely V2G technology, enables the utilization of EVs as distributed energy storage systems. This technology can provide many services in DC MGs such as steady-state power balancing (e.g., peak shaving) and voltage regulation [27]. In steady-state power balancing, the effective utilization of EVs calls for proper optimal energy management and scheduling technique. On the other hand, in voltage regulation services, EVs are deployed to improve the transient response and voltage quality of MG which in turn requires the implementation of real-time energy management systems (EMSs) and suitable primary controllers [28]. However, the existing methods for short-term utilization of EVs (e.g., for MG voltage regulation), may lead to frequent charge/discharge of the EVs' internal BESSs, thereby reducing the EV range and diminishing their BESSs lifetime. Besides, in these methods, each EV is considered to be a distributed BESS, so the deployment of the internal SC of modern EVs with HESS technologies cannot be provided.

The goal of this paper is to effectively employ the internal SC of modern EVs with HESS technologies to not only improve the lifetime of EV's BESS but also to absorb the instantaneous power variation of the RESs and loads in an islanded building-level DC MG for increasing the lifetime of the MG's CBESS and to enhance the transient response and voltage stability of the MG. In other words, instead of installing an SC to expand the lifetime of the grid-forming CBESS of the DC MG and improve its performance, this paper develops a novel EV charging method to utilize the internal SC of modern EVs to coordinate with CBESS during the islanded mode of the DC MG, so that 1) expand the CBESS's lifetime, and 2) enhance dynamic stability and voltage quality of the system. The realization of this plan requires to design of effective coordination between the internal SC of EVs and the MG's CBESS. To provide this coordination, understanding the internal power allocation strategy of each EV is also essential. For instance, if the absorbed power by an EV contains some high-frequency components which are not filtered by the EV's power smoothing filter, the BESS of the EV may be degraded. Nevertheless, the internal power allocation strategy of EVs is unknown to the MG control and management system. Therefore, a correct estimation of the EVs' internal power allocation systems is essential. To address the discussed challenges, this paper has the following contributions:

- This paper proposes and develops the idea of utilizing the internal SC of modern EVs with HESS technologies to improve the transient voltage quality in islanded building-level DC MGs as well as enhance the lifetime of the MGs' CBESS without degrading the internal BESS of the EVs.
- An online system identification technique is proposed to estimate the internal power allocation strategy of EVs. This approach is based on the parametric identification of an ARX model. To this end, an RLS algorithm is applied which is governed by a forgetting factor. This estimation is then used to provide effective coordination between the CBESS of the MG and the internal SC of EV.
- A filtration-based current allocation between the EV and MG's CBESS is proposed in which the high-frequency power variations of RESs and loads are assigned to the SC of the EV while the internal BESS of the EV is charging with its standard current profile. Therefore, the output power/current of the CBESS of the MG is smoothed without impacting the charging profile of the EV's BESS.
- A small signal stability analysis is proposed to investigate the impact of the proposed EV charging method on the transient voltage stability of the DC MG. The stability analysis results indicate that the marginal voltage stability of the DC MG is improved during the charging process of the EV with the proposed approach. Therefore, when the EV is charging, the MG voltage controller can operate with considerably larger gain values leading to better transient

This article has been accepted for publication in IEEE Transactions on Sustainable Energy. This is the author's version which has not been fully edited and content may change prior to final publication. Citation information: DOI 10.1109/TSTE.2023.3254597

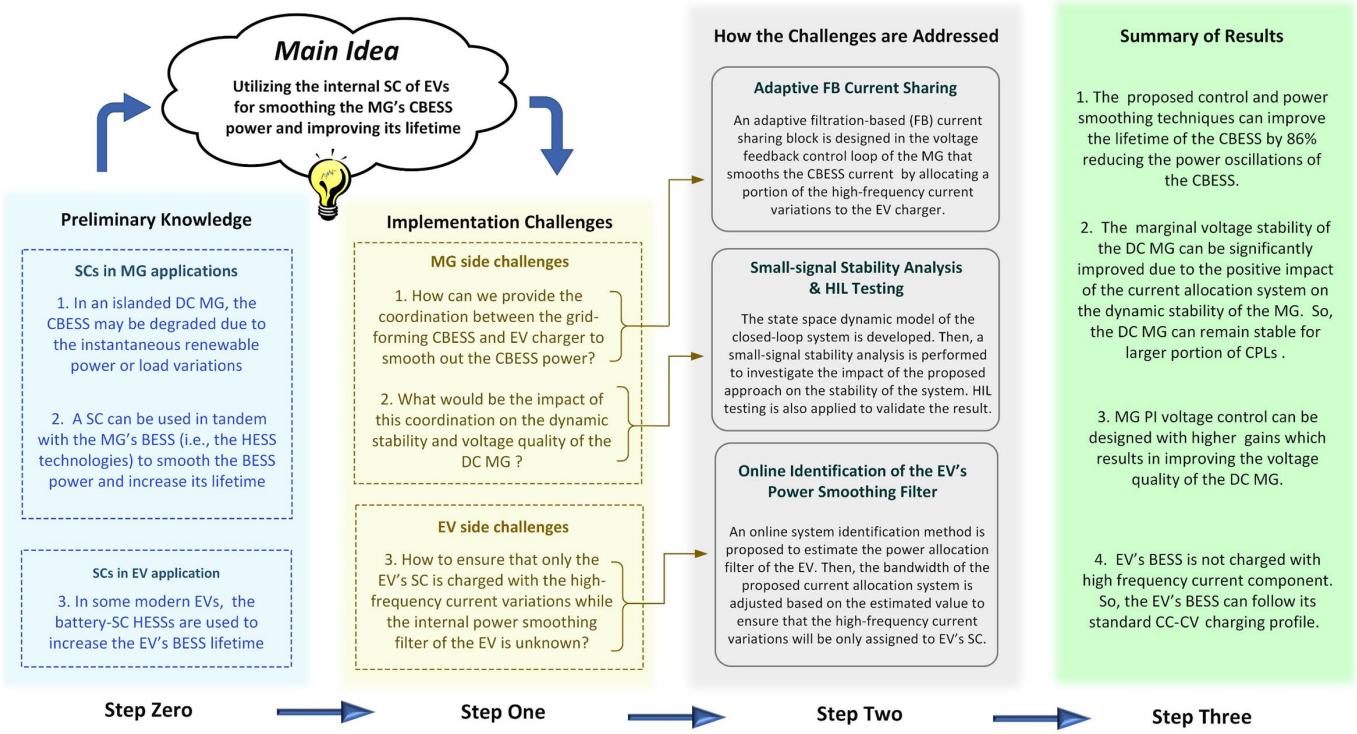

Fig. 1. Step-by-step implementation of this work.

response and voltage quality. Moreover, using the proposed EV charging method, a conventional PI voltage control can guarantee a high stability margin while the DC MG is loaded by a large CPL. These results are also experimentally verified by deploying a HIL testing.

- The simulation results show that the CBESS power variation is 86% reduced in a case study system by using the proposed EV charging method without impacting the constant charging profile of the EV's BESS. Also, the HIL testing results show that voltage quality can be improved by reducing 87% of the amplitude and decreasing 56% of the settling time of the transient voltage deviations in a specific load change scenario.

The step-by-step implementation of this work is illustrated in Fig. 1. It should be noted that this paper only focuses on the islanded operation of the building-level DC MGs because the CBESS degradation and voltage stability issues are more serious in the islanded mode of the system compared to the grid-connected mode. In this regard, one can assume that the DC MG controllers and EV chargers follow their conventional settings during the grid-connected mode of the system. The rest of this paper is organized as follows: Section II overviews the structure of the proposed control and management system and summarizes the assumptions and objectives of this work. Section III proposes the online system identification technique. Section IV discusses the impact of the proposed EV charging on the dynamic voltage stability of the DC MG. Section V validates the performance of the proposed technique using computer simulation and hardware-in the- loop (HIL) testing. Section VI discusses the limitation and future research direction, and Section VII concludes the paper.

II. System Overview

Fig. 2 represents the case study system in this work. This system is an islanded low-voltage DC MG that contains a CBESS, a PV module, a resistive load and a group of AC, and DC CPLs. The CBESS operates as the master or grid-forming unit and is responsible for voltage regulation and maintaining the power balance inside the system. The PV module operates in MPPT mode. This paper has also the following assumptions:

- The case study system is a small-scale DC MG with a single bus configuration that serves a commercial building with a 100kW nominal load. In this system, the load and DERs (i.e., CBESS, PV , and EVs) are located in close proximity to each other. Therefore, the impact of cable parameters (i.e., line impedances) is fairly negligible.
- It is assumed that each EV utilizes a semi-active battery-supercapacitor HESS which is the common HESS topology in EV applications [25]. Also, it incorporates a conventional power smoothing filter that is supervised by a rule-based EMS to perform the power/current assignment between the EV's BESS and SC.
- The internal power allocation strategy of EVs (i.e., the bandwidths of the power smoothing filter) is unknown. In addition, the MG control system cannot directly perform the power allocation between the BESS and SC of an EV.
- It is assumed that CBESS is efficiently sized. So, there is no need to employ the energy storage capacity of the EVs' BESSs to maintain the balance between PV power generation and loads (e.g., for peak shaving). Consequently, the EVs' BESSs can follow their standard charging profile during the connection to the EV chargers. Hence, this work only focuses on the effective utilization of the internal SC of EVs for

This article has been accepted for publication in IEEE Transactions on Sustainable Energy. This is the author's version which has not been fully edited and content may change prior to final publication. Citation information: DOI 10.1109/TSTE.2023.3254597

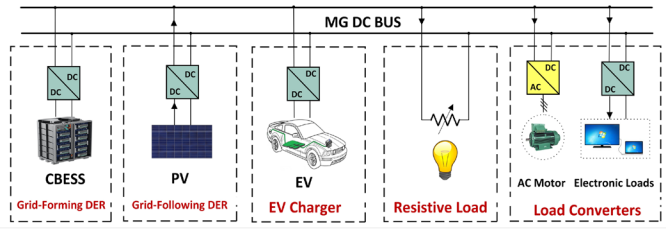

Fig. 2. The schematic model of the case study DC MG (i.e., an islanded small-scale DC MG with single bus configuration).

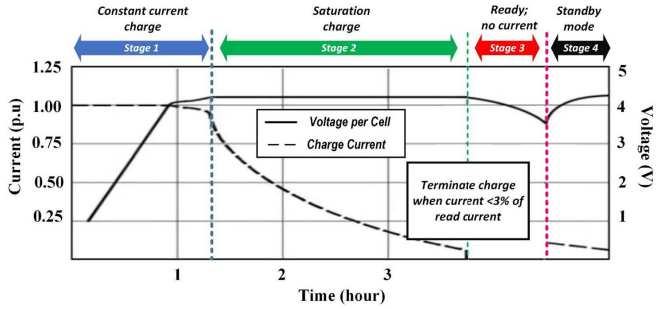

Fig. 3. CC–CV charge stages for the EV's BESS adopted from [29].

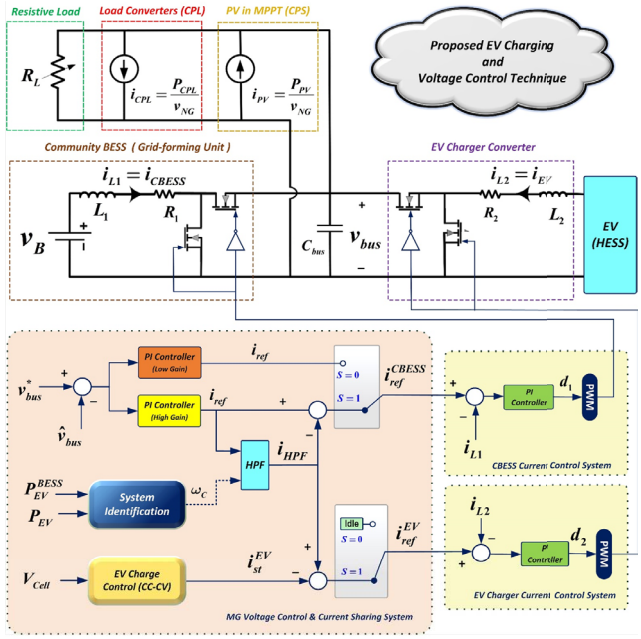

Fig. 4. The control structure and circuit model of the case study DC MG.

absorbing the instantaneous power fluctuation generated by the loads and PV.

- The charging profile of the EV's BESS is based on a standard constant current-constant voltage (CC-CV) approach represented in Fig. 3 [29]. This charging process begins with a constant current until a certain voltage value, known as the high voltage limit, is reached. Assuming that EV utilizes a Li-ion battery with the cathode materials of cobalt, nickel, manganese, and aluminum, the high voltage limit is selected as 4.20V per cell.

Fig. 4 shows the control structure and circuit model of the case study DC MG. As seen, the CBESS operates as the gird-forming unit of the system to regulate the DC bus voltage. To this end, the PI voltage controller of the MG computes a reference current (i.e., i_{ref}). When there is no EV connected to the charger, the EV charger is in idle mode (i.e., $S=0$). In this case, i_{ref} is directly sent to the CBESS's current controller which is similar to the conventional control strategy of DC MGs. On the other hand, when the EV is connected to the EV charger (i.e., $S=1$), i_{ref} is sent to the current/power allocation system. This system subtracts the high-frequency components of i_{ref} to smooth out the output current of the CBESS and then adds the high-frequency components to the output current of the EV charger. Therefore, the internal SC of the EV is utilized for absorbing transient power fluctuations as well as MG voltage regulation. The cut-off frequency (i.e., ω_c) of the high-pass filter (HPF) is adjusted based on the estimated dynamic model of the power allocation system of the EV's HESS so that charging the internal BESS of the EV with high-frequency components of i_{ref} is avoided. In another word, the MGs' current allocation system effectively adjusts the filter's bandwidth to guarantee that the high-frequency variation of RESs or loads is only absorbed by the internal SC of the EV.

III. Estimating the Parameters of the EVs' Power Management Systems

Practically, different brands of EVs may have different internal power management systems. On the other hand, the internal power allocation strategy of an EV is unknown for the MG control system. Therefore, an online estimation of the EVs' power allocation system is needed to provide effective coordination between the CBESS and EV. To this end, the DC MG utilizes an input-output system identification approach to estimate the internal power allocation strategy of the EV. The structure of this method is illustrated in Fig. 5. This estimation is based on an online parametric identification of an ARX model. The choice of this method can be justified by the fact that it is simple to implement. In addition, it is assumed that the EV utilizes a conventional semi-active HESS topology in which the BESS is directly connected to the EV DC link and SC is connected through a bidirectional DC to DC converter that is in current control mode (see Fig. 5). In this configuration, the high-frequency current variations of the HESS are assigned to the SC using a power allocation filter through adjusting reference current of the SC's converter (i.e., i_{ref}^{SC}). In addition, the EV utilizes a rule-based EMS to avoid overcharging/discharging of the SC during acceleration of the car with very high-power rates. However, it will not react when the EV is charging due to the relatively low amplitudes of high-frequency current variations. Therefore, the purpose of the proposed system identification is to estimate which range of frequencies are filtered by the SC and its power filtering system.

As seen in Fig. 5, the online system identification module measures P_{EV} and P_{EV}^{BESS} at each sampling time (i.e., T_s) in the EV charging spot. Then, an ARX model is fitted to the data as

$$A(q^{-1})y_t = B(q^{-1})u_t + e_t \quad (1)$$

where $y_t = P_{EVi}^{bat}$, $u_t = P_{EVi}$, and e_t is the prediction error. Also,

This article has been accepted for publication in IEEE Transactions on Sustainable Energy. This is the author's version which has not been fully edited and content may change prior to final publication. Citation information: DOI 10.1109/TSTE.2023.3254597

$A(q^{-1}) = 1 + a_1 q^{-1}$ and $B(q^{-1}) = b_0 + b_1 q^{-1}$ that yields

$$G(q^{-1}) = \frac{B(q^{-1})}{A(q^{-1})} = \frac{b_0 + b_1 q^{-1}}{1 + a_1 q^{-1}} \tag{2}$$

This model can be written in the linear regression form as

$$y_t = \lambda^T \varphi_t + e_t \tag{3}$$

where φ_t^T and λ^T are

$$\varphi_t^T = \left(-y_{t-1}, u_t, u_{t-1}\right), \quad \lambda^T = (a_1, b_0, b_1) \tag{4}$$

To estimate the parameters of the ARX model (i.e., a_1, b_0, and b_1), a recursive least squares algorithm with a gradient-based forgetting factor is utilized. This approach is discussed in detail in [30]. Consequently, the system identification may continuously update the estimated parameters during system operation that can provide a more accurate linear time-invariant (LTI) approximation of the EV's internal power allocation system.

Now, consider an LTI first-order analog filter. The transfer function of this filter can be represented in Laplace form as

$$H_{LPF}^{EV}(s) = \frac{\omega_H}{s + \omega_H} \tag{5}$$

where ω_H is the corner frequency of the LTI low-pass filter. The equivalent digital filter in the Z-domain can be also obtained as

$$H_{LPF}^{EV}(z) = \frac{z-1}{z} Z\left(\mathcal{L}^{-1}\left(\frac{H(s)}{s}\right)\right) = \frac{1 - e^{-\omega_H T_s}}{z - e^{-\omega_H T_s}} \tag{6}$$

Considering (1) to (6), the corner frequency of the LTI low-pass analog filter can be approximated as

$$\omega_H^* = -\frac{1}{T_s}\ln(-a_1) \tag{7}$$

where a_1 is the estimated parameter defined in (4). Moreover, in the initialization step of the algorithm (i.e., the initial guess of the filter parameters) b_0 and b_1 are considered as $b_0 = 0$, and $b_1 = 1 + a_0$. So, it can be shown that by running the online system identification algorithm, these parameters are computed as $b_0 \simeq 0$, $b_1 \simeq 1 - e^{-\omega_H T_S}$. In the next step, to guarantee that the high-frequency variation of i_{ref} is not assigned to the internal BESS of the EV, the estimated cut-off frequency should be smaller than the cut-off frequency of the HPF (i.e., $\omega_H^* < \omega_c$). In addition, to reduce transient variations on the HPF bandwidth, the estimated value for the HPF cut-off frequency is smoothed through a low-pass linear filter. So, the cut-off frequency of the HPF in the MG current allocation system is defined as

$$\eta \frac{d\omega_c}{dt} + \omega_c = K_f \omega_H^*, \; K_f > 1, \; \eta > 0 \tag{8}$$

where K_f is a constant value (i.e., the filtering constant) that should be defined enough large to guarantee that only the EV's SC will be charged by high-frequency current variations, and η is the time constant of the LPF.

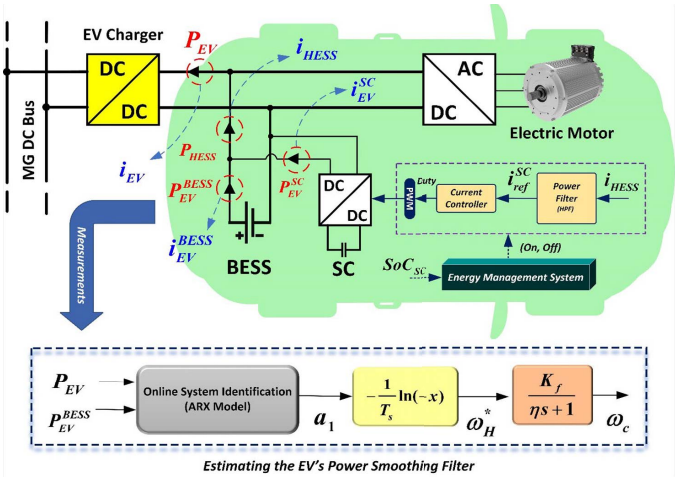

Fig. 5. The structure of the proposed system identification approach. .

IV. Stability Analysis

This section discusses the impact of the proposed EV charging method on the transient voltage stability of the system. To this end, the state-space dynamic model of the closed-loop system is developed. Then, the small-signal stability of the system in conventional and proposed EV charging methods is compared using the eigenvalue analysis of the linearized dynamic model of the system.

A. Dynamic Modeling

Based on the circuit model of the system shown in Fig. 4, and by considering the averaged dynamic model of the power electronic converters, the open-loop dynamic model of the system is obtained as

$$\begin{cases} L_1 \dfrac{di_{L1}}{dt} = v_{bat} - R_1 i_{L1} - v_{bus}(1 - d_1) \\ L_2 \dfrac{di_{L2}}{dt} = v_{EV} - R_2 i_{L2} - v_{bus}(1 - d_2) \\ C_{bus} \dfrac{dv_{bus}}{dt} = i_{L1}(1 - d_1) + i_{L2}(1 - d_2) + \dfrac{(P_{PV} - P_{CPL})}{v_{bus}} - \dfrac{v_{bus}}{R_L} \end{cases} \tag{9}$$

where i_{L1} and i_{L2} represent the inductor or the output currents of the CBESS and EV's HESS. R_1 and R_2 are the resistance, and L_1 and L_2 are the inductance of the CBESS and EV charger power electronic converters, respectively. Moreover, C_{bus} is the equivalent capacitance of the MG DC bus and v_{bus} represents the DC bus voltage. Also, R_L is the total resistive load of the system and P_{CPL} is the demanded power of by CPLs. The PV power generation is also represented by P_{PV}. Assuming the PV unit operates in maximum power point tracking (MPPT) mode, it behaves like a constant power source. Furthermore, d_1 and d_2 are the duty cycle of the CBESS and EV charger converters and they are obtained as

This article has been accepted for publication in IEEE Transactions on Sustainable Energy. This is the author's version which has not been fully edited and content may change prior to final publication. Citation information: DOI 10.1109/TSTE.2023.3254597

$$\begin{cases} \dfrac{dx_{\text{int}1}}{dt} = i_{ref}^{CBESS} - i_{L1} \\ \dfrac{dx_{\text{int}2}}{dt} = i_{ref}^{EV} - i_{L2} \\ d_1 = K_{P1}(i_{ref}^{CBESS} - i_{L1}) + K_{I1}x_{\text{int}1} \\ d_2 = K_{P2}(i_{ref}^{EV} - i_{L2}) + K_{I2}x_{\text{int}2} \end{cases} \tag{10}$$

where $x_{\text{int}1}$ and $x_{\text{int}2}$ are the integral of the error between the reference currents and the inductor currents of the converters. Also, the pairs of (K_{P1}, K_{I1}) and (K_{P2}, K_{I2}) show the proportional and integral gains of the current controllers. Moreover, i_{ref}^{EV} and i_{ref}^{CBESS} show the reference currents of the EV charger and CBESS power electronic converters, respectively, which are computed by the MG voltage control and current sharing system (see Fig. 4). Then, let us assume that the HPF is a first-order linear-time-invariant (LTI) filter that has the following transfer function in Laplace form.

$$H_{HPF}(s) = \frac{\tau_c s}{\tau_c s + 1} \tag{11}$$

where $\tau_c = (\omega_c)^{-1}$ is the time constant of the HPF and ω_c is obtained using (1) to (8) (also see Fig. 5). Then, i_{ref}^{CBESS} and i_{ref}^{EV} are obtained as

$$\begin{cases} \dfrac{dx_{\text{int}v}}{dt} = v_{MG}^{*} - \hat{v}_{bus} \\ \tau_c \dfrac{dx_f}{dt} = -x_f + K_{Iv}x_{\text{int}v} + K_{pv}\left(v_{bus}^{*} - \hat{v}_{bus}\right) \\ i_{ref}^{CBESS} = x_f \\ i_{ref}^{EV} = K_{Iv}x_{\text{int}v} - x_f + K_{Pv}\left(v_{bus}^{*} - \hat{v}_{bus}\right) - i_{st}^{EV} \end{cases} \tag{12}$$

where $x_{\text{int}v}$ and x_f are the dynamic states of the voltage controller and current assignment filter, respectively, and i_{st}^{EV} is the standard charging current of the EV. The pair of (K_{Pv}, K_{Iv}) shows the proportional and integral gains of the PI voltage controller. In addition, v_{bus}^{*} is the nominal voltage of the MG DC bus and $\hat{v}_{bus}$ is the measured voltage at the MG DC bus. Assuming the voltage measurements has τ_d time delay, and using a first-order Pade approximation of the delay, $\hat{v}_{dc}$ is obtained as

$$\begin{cases} \dfrac{1}{2}\tau_d \dfrac{dx_d}{dt} = -x_d + v_{bus} \\ \hat{v}_{bus} = 2x_d - v_{bus} \end{cases} \tag{13}$$

where x_d is the dynamic state of the delay. Considering (9) to (13), the dynamic model of the closed-loop system can be represented in a state-space form as

$$\dot{x} = f(x, u, w) \tag{14}$$

where $x^T = [i_{L1}, i_{L2}, v_{bus}, x_f, x_d, x_{\text{int}1}, x_{\text{int}2}, x_{\text{int}v}]$ is the set of dynamic states of the closed-loop system, $u = v_{MG}^{*}$ is the reference input and $w = [P_{CPL}, P_{PV}, i_{st}^{EV}, v_{bat}, v_{EV}]^T$ is the set of disturbances.

By considering (9) to (14), the nonlinear state-space dynamic model of the closed-loop system is obtained as (15). It should be noted that based on (11), if $\tau_c \to 0$, then $x_f = i_{ref}$, $i_{ref}^{CBESS} = i_{ref}$, and $i_{ref}^{EV} = i_{st}^{EV}$. This means that the dynamic model of the DC MG with conventional EV charging method can be obtained from (12) to (15) by considering $\tau_c \simeq 0$.

$$\begin{bmatrix} \dfrac{di_{L1}}{dt} \\ \dfrac{di_{L2}}{dt} \\ \dfrac{dv_{bus}}{dt} \\ \dfrac{dx_f}{dt} \\ \dfrac{dx_d}{dt} \\ \dfrac{dx_{\text{int}1}}{dt} \\ \dfrac{dx_{\text{int}2}}{dt} \\ \dfrac{dx_{\text{int}v}}{dt} \end{bmatrix} = \begin{bmatrix} \dfrac{1}{L_1}v_{bat} - \dfrac{R_1}{L_1}i_{L1} - \dfrac{1}{L_1}v_{bus} + \dfrac{K_{P1}}{L_1}v_{bus}x_f \\ -\dfrac{K_{P1}}{L_1}v_{bus}i_{L1} + \dfrac{K_{I1}}{L_1}v_{bus}x_{\text{int}1} \\ \dfrac{1}{L_2}v_{EV} - \dfrac{R_2}{L_2}i_{L2} - \dfrac{1}{L_2}v_{bus} + \dfrac{K_{P2}K_{Pv}}{L_2}v_{bus}^{*}v_{bus} \\ -\dfrac{2K_{P2}K_{Pv}}{L_2}v_{bus}x_d + \dfrac{K_{P2}K_{Pv}}{L_2}v_{bus}^{2} + \dfrac{K_{P2}K_{Iv}}{L_2}v_{bus}x_{\text{int}v} \\ -\dfrac{K_{P2}}{L_2}v_{bus}x_f - \dfrac{K_{P2}}{L_2}v_{bus}i_{L2} + \dfrac{K_{I2}}{L_2}v_{bus}x_{\text{int}2} - \dfrac{K_{P2}}{L_2}v_{bus}i_{st}^{EV} \\ \dfrac{1}{C_{bus}}i_{L1} - \dfrac{K_{P1}}{C_{bus}}x_f i_{L1} + \dfrac{K_{P1}}{C_{bus}}i_{L1}^{2} - \dfrac{K_{I1}}{C_{bus}}i_{L1}x_{\text{int}1} + \dfrac{1}{C_{bus}}i_{L2} \\ -\dfrac{K_{P2}K_{Pv}}{C_{bus}}v_{bus}^{*}i_{L2} + \dfrac{2K_{P2}K_{Pv}}{C_{bus}}x_d i_{L2} - \dfrac{K_{P2}K_{Pv}}{C_{bus}}v_{bus}i_{L2} \\ -\dfrac{K_{P2}K_{Iv}}{C_{bus}}i_{L2}x_{\text{int}v} + \dfrac{K_{P2}}{C_{bus}}i_{L2}x_f + \dfrac{K_{P2}}{C_{bus}}i_{L2}^{2} - \dfrac{K_{I2}}{C_{bus}}i_{L2}x_{\text{int}2} \\ +\dfrac{K_{P2}}{C_{bus}}i_{L2}i_{st}^{EV} + \dfrac{(P_{PV} - P_{CPL})}{C_{bus}v_{bus}} - \dfrac{1}{C_{bus}R_L}v_{bus} \\ -\dfrac{1}{\tau_c}x_f + \dfrac{K_{Pv}}{\tau_c}v_{bus}^{*} - \dfrac{2K_{Pv}}{\tau_c}x_d + \dfrac{K_{Pv}}{\tau_c}v_{bus} + \dfrac{K_{Iv}}{\tau_c}x_{\text{int}v} \\ -\dfrac{2}{\tau_d}x_d + \dfrac{2}{\tau_d}v_{bus} \\ x_f - i_{L1} \\ K_{Pv}v_{bus}^{*} - 2K_{Pv}x_d + K_{Pv}v_{bus} + K_{Iv}x_{\text{int}v} - x_f - i_{L2} - i_{st}^{EV} \\ v_{bus}^{*} - 2x_d + v_{bus} \end{bmatrix} \tag{15}$$

B. Eigen-value Analysis

This section investigates the marginal voltage stability of DC MG under the proposed EV charging method and compares it with the conventional charging method of EVs in low-voltage DC MGs. To this end, the small-signal stability of the DC MGs is measured by analyzing the eigenvalues of the linearized systems. The theorems related to the time-delay eigenvalue analysis are discussed in details in [31]. The selection of this

method can be justified due to the high complexity of the nonlinear model of the closed-loop system.

Let us consider the nonlinear state-space dynamic model of the DC MGs represented in (14) and (15). The equilibrium points of the system (i.e., $(\bar{x},\bar{u},\bar{w})$) can be found as

$$\dot{\bar{x}} = 0 \Leftrightarrow f(\bar{x},\bar{u},\bar{w}) = 0 \tag{16}$$

Using a first-order Taylor series expansion of f , and defining $\delta x = x - \bar{x}$, $\delta u = u - \bar{u}$, and $\delta w = w - \bar{w}$ one can obtain:

$$\delta\dot{x} = \dot{x} - \dot{\bar{x}} = f(x,u,w) \simeq A_{|(\bar{x},\bar{u},\bar{w})}\delta x + B_{|(\bar{x},\bar{u},\bar{w})}\delta u + D_{|(\bar{x},\bar{u},\bar{w})}\delta w \tag{16}$$

where A, B , and D are defined as

$$A_{|(\bar{x},\bar{u},\bar{w})} = \left.\frac{\delta f(x,u,w)}{\delta x}\right|_{(\bar{x},\bar{u},\bar{w})} \tag{17}$$

$$B_{|(\bar{x},\bar{u},\bar{w})} = \left.\frac{\delta f(x,u,w)}{\delta u}\right|_{(\bar{x},\bar{u},\bar{w})} \tag{18}$$

$$D_{|(\bar{x},\bar{u},\bar{w})} = \left.\frac{\delta f(x,u,w)}{\delta w}\right|_{(\bar{x},\bar{u},\bar{w})} \tag{19}$$

Therefore, to compute the closed-loop poles of the linearized system at each operating point, it is needed to determine the eigenvalues of the Jacobian matrix (i.e., A).

To evaluate the impact of the proposed EV charging method on the transient voltage stability of the system, two case-study DC MGs are compared. In the first case, the DC MG utilizes a conventional EV charging method. On the other hand, the second case study DC MG uses the proposed EV charging method illustrated in Fig. 4. The parameters of the case study DC MGs are given in Table I. Because the CPS and resistive load have a positive impact on the marginal voltage stability of the DC MGs [10], it is assumed that the PV power generation is less than 20% of its nominal value (i.e., $P_{PV} = 10\text{kW}$) and the resistive load is very small (i.e., $R_L = 100\Omega$), so that the marginal stability of the DC MG in severe stability conditions (i.e., small CPS, low resistive load, and large CPLs) can be evaluated.

TABLE I
SYSTEM PARAMETERS

Symbol	Quantity	Value
v_{bus}^{*}	Reference or nominal voltage of the DC bus	200V
K_{P1}, K_{P2}	Proportional gains of the current regulators	200
K_{I1}, K_{I2}	Integral gains of the current regulators	500
L_1, L_2	Inductance of the converter filter	500μH
R_1, R_2	Resistance of the converter filter	200mΩ
C_{bus}	Total capacitance of the MG dc bus	8mF
v_{bat}	Terminal voltage of CBESS	50V
v_{EV}	Terminal voltage of EV's BESS (or HESS)	40V

Fig. 6 shows the dominant poles of the closed-loop system in the case study DC MGs based on different values of the proportional gain of the PI voltage controller (i.e., K_{Pv}). In this experiment, both DC MGs supply relatively large CPLs. As seen in Fig.6(a), the closed-loop poles of system move to the unstable region by increasing the K_{Pv} in a DC MG with the conventional voltage control and EV charging method, and the voltage controller will be destabilized for $K_{Pv} > 2.9$. However, using the proposed EV charging method, the DC MG can remain stable for remarkably larger values of K_{Pv} representing the higher stability margin of the MG voltage controller. Similarly, as seen in Fig. 7, the voltage controller can remain stable for considerably larger values of the integral gain (i.e., K_{Iv}) with the proposed EV charging approach. Fig. 8 studies the impact of the communication delay (i.e., τ_d) in both case study DC MGs. As seen, the MG's voltage control system will be destabilized for $\tau_d > 3.9\text{ms}$ in DC MG with the conventional EV charging method. However, the DC MG can remain stable for significantly larger delays (i.e., $\tau_d < 30\text{ms}$) in the proposed approach due to the higher stability margin of the voltage controller. Fig. 9 shows the impact of the CPLs on the dynamic voltage stability of the DC MG. As seen, in conventional method, the DC MG will be destabilized for $P_{CPL} > 66\text{kW}$. However, the PI voltage controller can tolerate remarkably larger

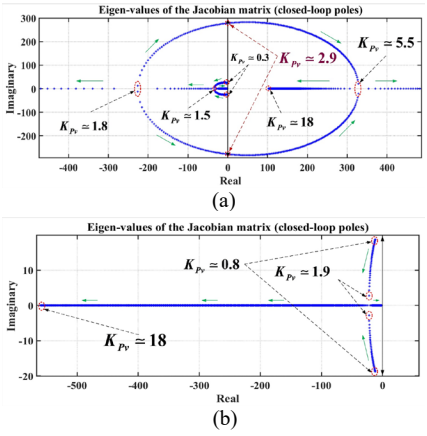

Fig. 6. Dominant poles of the closed-loop system with respect to different values of K_{Pv}, (a) the conventional technique, (b) the proposed approach. Also, $P_{CPL} = 60\text{kW}$, $P_{PV} = 10\text{kW}$, $i_{st}^{EV} = 40\text{A}$, $\tau_c = 0.5\text{s}$, $K_{Iv} = 20$, and $\tau_d = 1\text{ms}$.

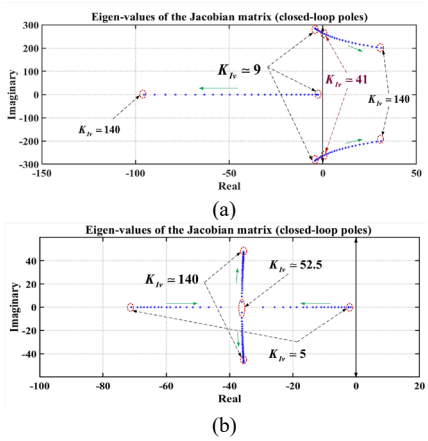

Fig. 7. Dominant poles of the closed-loop system with respect to different values of K_{Iv}, (a) the conventional technique, (b) the proposed approach. Also, $P_{CPL} = 60\text{kW}$, $P_{PV} = 10\text{kW}$, $i_{st}^{EV} = 40\text{A}$, $\tau_c = 0.5\text{s}$, $K_{Pv} = 2.5$, and $\tau_d = 1\text{ms}$.

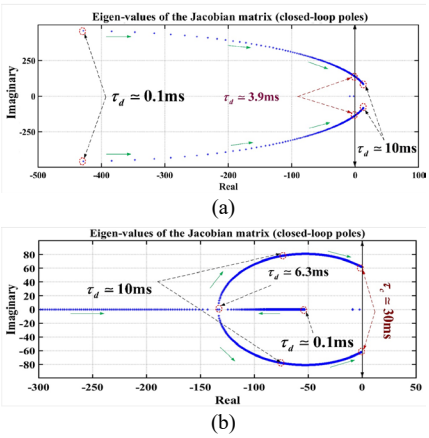

Fig. 8. Dominant poles of the closed-loop system with respect to different values of τ_d, (a) the conventional technique, (b) the proposed approach. Also, $P_{CPL} = 60\text{kW}$, $P_{PV} = 10\text{kW}$, $i_{st}^{EV} = 40\text{A}$, $\tau_c = 0.5\text{s}$, $K_{Pv} = 2.5$, and $K_{Iv} = 20$.

This article has been accepted for publication in IEEE Transactions on Sustainable Energy. This is the author's version which has not been fully edited and content may change prior to final publication. Citation information: DOI 10.1109/TSTE.2023.3254597

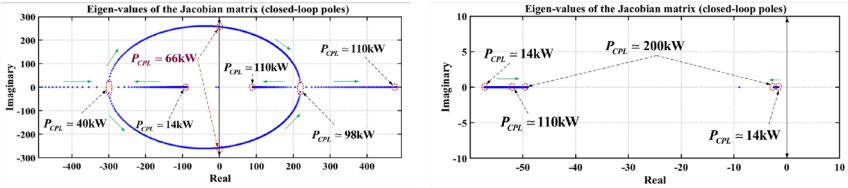

(a) (b)

Fig. 9. Dominant poles of the closed-loop system with respect to different values of P_{CPL}, (a) the conventional technique, (b) the proposed EV charging approach. Also, $P_{PV} = 10\text{kW}$, $i_{st}^{EV} = 80\text{A}$, $\tau_c = 0.5\text{s}$, $\tau_d = 1\text{ms}$, $K_{PV} = 2.5$, and $K_{Iv} = 20$.

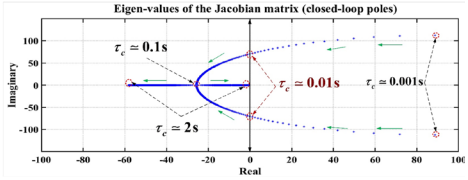

Fig. 10. Dominant poles of the closed-loop system with respect to different values of τ_c. Also, $i_{st}^{EV} = 40\text{A}$, $P_{CPL} - P_{PV} = 100\text{kW}$, $K_{Pv} = 2.5$, $K_{Iv} = 20$, and

CPL values in the proposed approach. This means that the instability effect of the CPLs that usually requires advanced voltage control techniques can be easily addressed by using the proposed EV charging technique.

The reason that the MG voltage controller has a higher stability margin in the proposed EV charging technique is indeed related to the impact of the current allocation filter (i.e., the HPF). As seen in Fig. 4 the reference current computed by the voltage controller passes through an HPF and then is added to the reference current of the EV charger to employ the internal SC of the EV for transient voltage regulation. In this structure, the HPF operates like a lead compensator which shifts the closed-loop poles of the DC MG to the left-hand side of the $j\omega$ axis (i.e., the stable region), thereby improving the marginal stability of the DC MG. This impact is illustrated in Fig. 10. As discussed, if $\tau_c \to 0$ the DC MG will have the same dynamic behavior to the conventional EV charging method. However, by increasing the filter's time constant (i.e., τ_c) the HPF provides a larger shift to the stable region and assigns a more portion of transient power fluctuations to the internal SC of the EV. Consequently, increasing the time constant of the HPF provides higher marginal stability for the DC MG.

V. Simulation Results

This section analyzes the impacts of the proposed EV charging method on the voltage quality and battery lifetime of the DC MGs. To this end, first, the power smoothing performance of the proposed approach as well as the accuracy of the system identification technique is evaluated using MATLAB/Simulink. Then, the performance of the proposed approach on the transient stability and voltage quality of DC MGs is analyzed using HIL testing.

A. Power Flow Analysis

To analyze the impact of the proposed approach on the lifetime of the CBESS (i.e., power smoothing performance) and investigate the power flow between the MG's CBESS and EV, the performances of the case-study DC MGs are compared using MATLAB/Simulink. The case study MGs have the following features:

- The first case study MG (i.e., Case 1) is a DC MG that utilizes the proposed EV charging method, and its circuit model and control structure is illustrated in Fig. 4.
- The second case study MG has a similar structure to the Case 1 system, but it utilizes a conventional EV charging method (i.e., the HPF is deactivated in Case 2).
- The corner frequency of the CBESS power smoothing filter (i.e., the HPF) is defined as 10 time larger than the estimated cut-off frequency of the EV power filtering system (i.e., $K_f = 10$) to guarantee that the high frequency current/power variations are only assigned to the EV's SC.
- The parameters of the DC MGs are illustrated in Table. 1. Also, it is assumed that $R_L = 100\Omega$.
- In both cases, the CBESS has 100kW nominal power and 2 hours of charge time. The EV's BESS has 12.8kW nominal charge/discharge power and 4 hours of charge time with 80A nominal charge current. The internal SC of the EV also has 50kW nominal power and 1s charge time.

In this experiment, the PV power generation and load profile in Case 1 are similar to those of Case 2. Fig. 11 shows the net power profile (i.e., P_{net}) of the case study systems for 10 minutes. The net power profile shows the difference between demanded power by the resistive load and CPLs and the generated power by the PV sources that can be represented as

$$P_{net} = P_{CPL} + \frac{v_{bus}^2}{R_L} - P_{PV} \tag{20}$$

Fig. 12 shows the estimated cut-off frequency of the EV internal power allocation system by the ARX model and the selected value for EV's CBESS current allocation system (i.e., the HPF) in Case 1 system. As seen, the proposed system identification provides an accurate estimation of the internal BESS-SC current assignment filter of the EV. As seen, the selected cut-off frequency for the HPF is defined as 10 times larger than the internal filter of the EV to guarantee that the high-frequency variations of the net power are not absorbed by the EV's BESS. In addition, due to the sudden load changes, the estimated value by the ARX model (i.e., ω_H^*) has some fast changes which are filtered by the designed first-order linear LPF to avoid undesirable transients. It should be noted that based on the selected cut-off frequency (i.e., $\omega_c = 0.2$), the HPF assigns almost all the instantaneous current ripples with frequencies higher than 1 rad/s or 0.16 Hz (i.e., $\omega > 5\omega_c$ or $f > 5f_c$) to the EV charger.

Fig. 13 and 14 depict the output power of the ESS units in Case 1 and Case 2 systems, respectively. In both cases, the EVs are in Stage 1 of their standard charging profile (see Fig. 4) in which the EV charges with a constant current/power. As seen in Fig. 14, in the conventional EV charging method, the EV's SC is useless, and it receives no power. However, in the proposed EV charging method (i.e., Case 1), the EV's SC absorbs the instantaneous power variation of the net power which smooths out the output power of

This article has been accepted for publication in IEEE Transactions on Sustainable Energy. This is the author's version which has not been fully edited and content may change prior to final publication. Citation information: DOI 10.1109/TSTE.2023.3254597

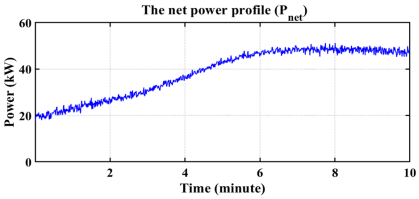

Fig. 11. The net power profile (i.e., P_{net}).

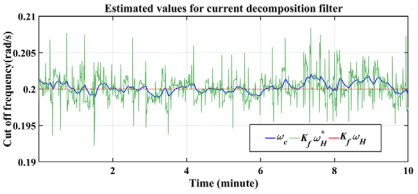

Fig. 12. The estimated cut off frequency values for CBESS-EV power/current allocation system ($\eta = 5, K_f = 10, \omega_H = 0.02, T_s = 1\text{ms}$).

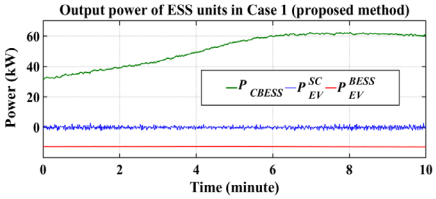

Fig. 13. The output power of the ESSs in Case 1 system (i.e., the proposed EV charging method).

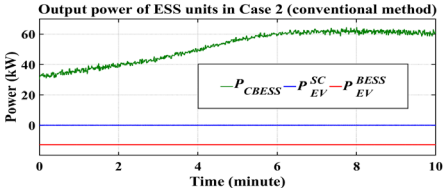

Fig. 14. The output power of the ESSs in Case 2 system (i.e., the conventional EV charging method).

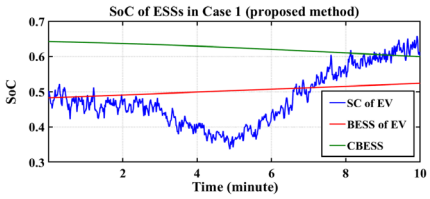

Fig. 15. SoC variation of the ESSs in the proposed EV charging method (i.e., Case 1).

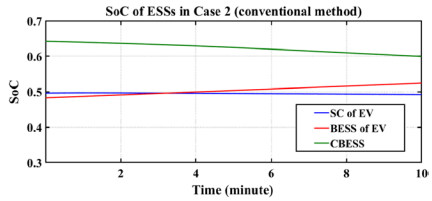

Fig. 16. SoC variation of the ESSs in the conventional EV charging method (i.e., Case 2).

TABLE II
POWER SMOOTHING ANALYSIS[1]

ESS	SAPV	
	Case 1	Case 2
CBESS	1.6 kW	11.7 kW
EV's BESS	0.02 kW	0.014 kW

[1] Case 1 is the proposed EV charging and Case 2 is the conventional method.

the CBESS. Therefore, as it can be seen in Fig. 13 and 14, the output power of the CBESS has considerably smoother variations in the proposed EV charging method compared to the conventional approach.

Fig. 15 and Fig. 16 illustrate the state of charge (SoC) variation of the ESS units in Case 1 and Case 2 systems, respectively. As seen, the SoC of CBESS and EV's BESS experience similar profiles in the Case 1 and Case 2 systems which means that the proposed approach does not impact the steady-state power and stored energy in batteries (i.e., CBESS and EV's BESS). On the other hand, the SoC of SC has completely different behaviors in Case 1 and Case 2 systems. The reason is that, in the conventional EV charging method, the SC does not absorb/release power, so its SoC almost remains unchanged. However, in the proposed EV charging approach the SoC of SC varies over time because it is utilized to absorb the high-frequency variations of the net power.

For quantified power smoothing analysis, the sum of absolute power variations (SAPV) is defined as

$$SAPV = \sum_{k} \left| P_{CBESS}(kT_s) - P_{CBESS}(kT_s - T_s) \right| \tag{21}$$

where T_s is the sampling time of the measurements. Considering $T_s = 1\text{ms}$, the SAPV can effectively show the CBESS power variations for frequencies less than 100Hz. So, it can cover all the high-frequency power variations caused by instantaneous renewable power fluctuations and sudden load shifts which mostly happen in 0.1 to 10 seconds time intervals (i.e., 0.1 to 10Hz). Then, the SAPVs of both cases are obtained based on the CBESS power profile in Case 1 and 2 shown in Fig. 13 and 14, respectively. This power smoothing comparison is shown in Table II indicating that the proposed EV charging method can reduce the CBESS power variations compared to the conventional technique by 86%. In addition, Table II shows that the power variations of the EV's BESS remain very small in the proposed approach meaning that EV's SC absorbs almost all the high-frequency power variations. So, since charging the Li-ion batteries with frequency power variations (or current ripples) can noticeably reduce their lifetime [7], [12], one can conclude that the proposed method can improve the CBESS lifetime without degrading the BESS of EVs.

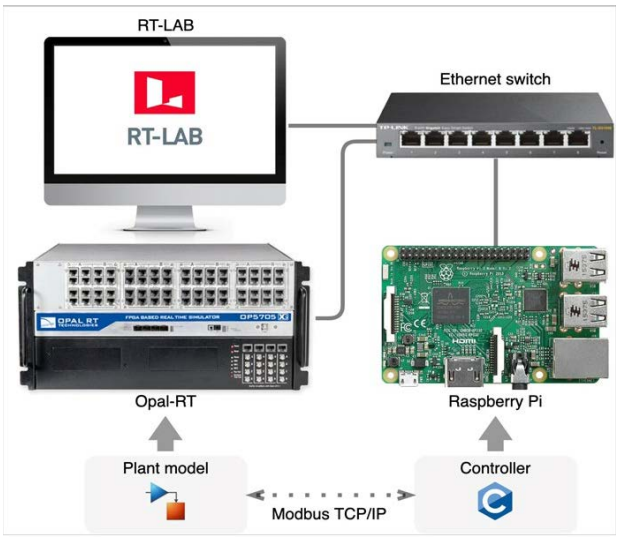

Fig. 17. The structure of the HIL testbed.

B. HIL Testing

The transient response and dynamic stability of the case study DC MGs (Case 1 and Case 2) are studied in a HIL testbed. The schematic of the HIL testbed is shown in Fig. 17. The testbed includes the real-time digital simulator, Opal-RT, and a microprocessor Raspberry Pi. RT-LAB installed host PC is used to run the DC MG's power system model in real time. The plant including the DC bus, power electronic converters, and current controllers is modeled in Simulink (see Fig. 4), and it runs in the Opal-RT via RT-LAB. The MG voltage control and current sharing system in Fig. 4 are developed in a C language script and run on the Raspberry Pi. The communications between all the hardware are established by an Ethernet connection. The MG controller receives the voltage

This article has been accepted for publication in IEEE Transactions on Sustainable Energy. This is the author's version which has not been fully edited and content may change prior to final publication. Citation information: DOI 10.1109/TSTE.2023.3254597

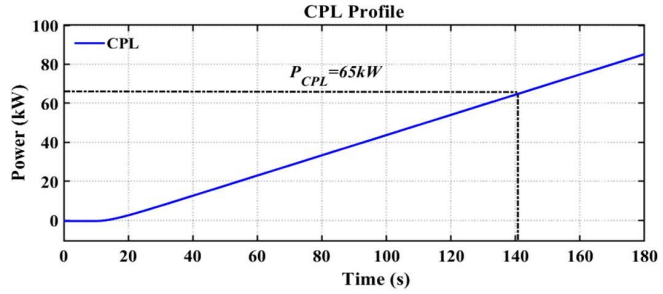

(a)

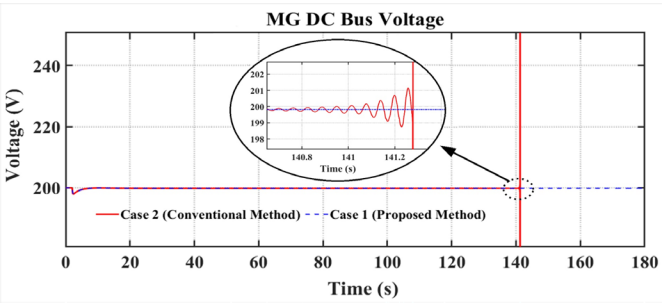

(b)

Fig. 18. CPL tolerance of the case study MGs. (a) CPL profile (b) MG DC bus voltage. In both cases, $P_{PV}=10\text{kW}$, $i_{st}^{EV}=40\text{A}$, $\tau_c=0.5\text{s}$, $\tau_d=1\text{ms}$, $K_{Pv}=2.5$, and $K_{Iv}=20$.

measurement from the plant and calculates the reference control inputs for the current controller of the converters, then sends them back to the plant via Modbus TCP/IP. The sampling time of the OPAL-RT simulator is $250\mu\text{s}$ and the action time of the Raspberry Pi controller is 1ms.

1) CPL Tolerance and Voltage Stability

In this section, to analyze the impact of the proposed EV charging method on the dynamic stability of the voltage control system, it is assumed that the voltage controllers have similar proportional and integral gains in Case 1 (i.e., the MG with the proposed EV charging method) and Case 2 (i.e., the MG with conventional EV charging method). In addition, the system parameters are exactly similar to the DC MGs that are compared in Fig. 9 for eigenvalue analysis in which $K_{Pv}=2.5$, $K_{Iv}=20$ and the PV has 10kW power generation. Also, there is a 1ms time delay between the real-time simulator (i.e., OPAL-RT) and the MG control system (i.e., the Raspberry Pi controller). In this experiment, the CPL value gradually increases in both cases to see which one of the case study systems becomes unstable sooner. Knowing the fact that the CPLs reduce the marginal stability of the DC MGs, the MG control strategy that provides higher CPL tolerance indicates a higher stability margin. As seen in Fig. 18, the DC bus voltage becomes unstable in the DC MG with the conventional EV charging method for CPLs larger than 65kW while the DC MG remains stable in the proposed EV charging method. This result also verifies the small-signal stability of the DC MGs provided in Fig. 9 in Section IV.B showing the eigenvalues of the closed-loop system move to the unstable region for CPLs larger than 66kW.

2) Transient Voltage Analysis

This section evaluates the transient voltage oscillations in the MG DC bus during sudden load changes. As discussed in the small-signal stability analysis of the DC MGs, the voltage controller can operate with larger gains in the DC MG with the proposed EV charging method due to its higher stability margin. In this respect, the gains of the voltage controller in Case 1 (i.e., the DC MG with proposed EV charging) are defined as $K_{Pv}=3.7$ and $K_{Iv}=80$. On the other hand, the gains of the voltage controller in Case 2 (i.e., the DC MG with conventional EV charging) are defined as $K_{Pv}=1.5$ and $K_{Iv}=20$ to avoid instability in large CPLs. Fig. 19 shows the transient response of the case study systems during sudden load changes (please also see the definition of i_{EV}, i_{CBESS}, i_{EV}^{BESS}, and i_{EV}^{SC} in Fig. 4 and 5). In both case study systems, it is assumed that the CBESS is responsible for MG voltage regulation and EV chargers are in constant current charging

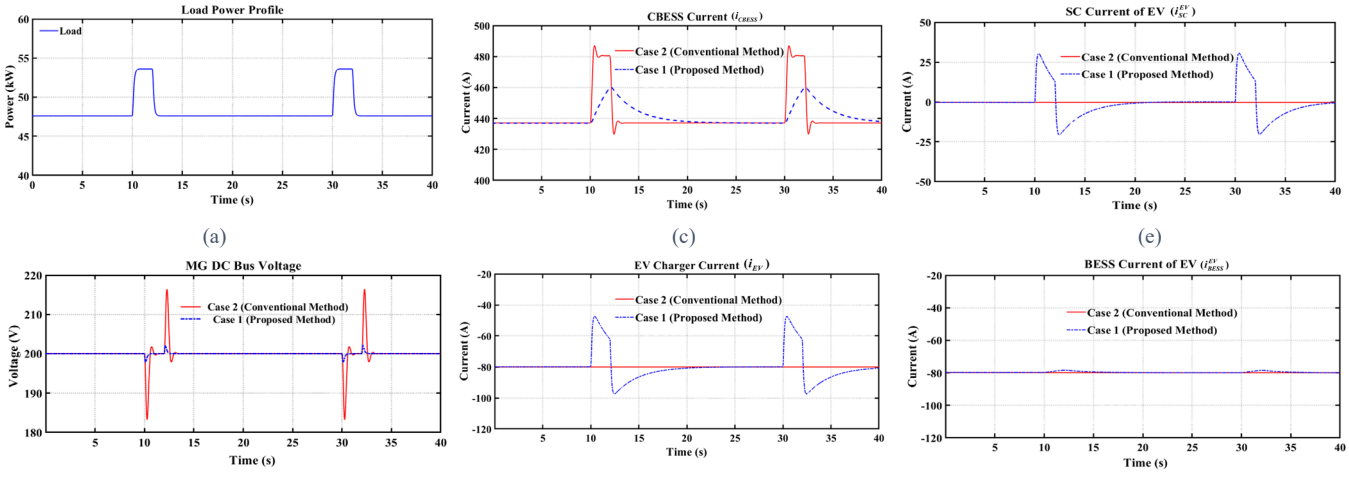

(a) (c) (e)

(b) (d) (f)

Fig. 19. Transient response analysis of the case study MGs. a) load power profile, b) DC bus voltage, c) CBESS current , d) EV charger current (i_{EV}), e) SC current of the EV's HESS (i_{SC}^{EV}). f) BESS current of the EV (i_{EV}^{BESS}). Nominal voltage is 200V and nominal load is 100kW.

TABLE III
TRANSIENT VOLTAGE DEVIATIONS IN A LOAD CHANGE[1]

Case	Amplitude (p.u)[2]	Settling Time (Error <0.01 p.u.)
Case 1	0.011 p.u	0.41s
Case 2	0.084 p.u.	0.93s

[1] Load steps up around 0.06 p.u. (see the load profile in Fig. 19 (a)).
[2] Nominal voltage is 200V and nominal load is 100kW.

mode to charge the EV's BESS with its nominal current (i.e., 80A). Also, the nominal voltage is 200V and the nominal load power is 100kW. In addition to this constant current, in the proposed EV charging method (see Fig. 4), the EV charger coordinates with the CBESS to supply the transient current/power during the sudden load changes. As seen in Fig. 19(b), the DC MG that utilizes the proposed EV charging method (i.e., Case 1) experiences significantly fewer transient voltage deviations during the sudden load changes compared to the DC MG with the conventional EV charging technique. In addition, it is clear that the CBESS experiences smoother current variations in Case 1 (the proposed EV charging method) because a large portion of the transient power/current variations are supplied by EV (see Fig 19(c) and (d)).

Fig. 19 (e) and (f) illustrate that using the proposed data-driven adaptive filtering technique, the transient/instantaneous current fluctuations are only absorbed by the internal SC of the EV. As a result, the charge current profile of the internal BESS of the EV remains constant which is similar to the conventional method for EV charging. Therefore, the proposed control structure and adaptive filtering technique can effectively utilize the internal SC of modern EVs with HESS technologies to supply the transient power/current oscillations without impacting the standard charging profile of the internal BESS of the EVs validating the power smoothing results in Table II. Table III also provides the quantified comparison between the proposed EV charging and the conventional method. As seen, the amplitude of the transient voltage deviations is decreased in Case 1 (i.e., the proposed approach) compared to the conventional method (i.e., Case 2) by around 87%. In addition, the time that is required for the DC bus voltage to settle again within 0.1 p.u. voltage error margin (i.e., $\left|v_{bus}^{*}-v_{bus}\right|<0.01$p.u.) is reduced using the proposed control structure and EV charging approach by 56%. Therefore, the proposed EV charging can noticeably improve the transient voltage quality of the system.

VI. DISCUSSION

The simulation results showed the superiority of the proposed MG control structure and EV charging method over the conventional technique in terms of reducing the CBESS power variations (i.e., fewer CBESS degradation) and higher transient voltage quality (i.e., the better response of the MG voltage control system). In addition, as it was shown in Section V, the key advantage of the proposed technique is that it does not impact the charging profile of the EVs' BESSs. This means that a building-level DC MG can take advantage of the proposed EV charging method without posing a cost to the EV owners by degrading the BESS of their EVs. However, the implementation of this technology may still have some practical challenges that need to be addressed. The main challenge is that in some cases, the owners of the building-level DC MG and EVs are different which may cause a conflict of interest. To address this issue, the DC MG owner can consider some incentives or discounts for EVs that are charged with the proposed EV charging method because of sharing their SC capacity with the DC MG. To determine the optimal amount of these incentives further studies are still needed. Therefore, a future research direction of this work can be the investigation of optimal incentives for the EVs that share their SC capacity with the DC MG using the proposed approach.

In addition, in this work, a conservative approach is used to adjust the bandwidth of the CBESS power smoothing filter with respect to the EV internal power filtering system. For instance, the corner frequency of the CBESS power smoothing filter is defined as 10 times larger than the estimated corner frequency of the EV's power filtering system. On the one hand, this conservative strategy is beneficial to simply guarantee that the high-frequency current variations of the RESs are only assigned to the EV's SC so that the EV's BESS is not degraded. On the other hand, a large portion (e.g., 30% to 50%) of the SC capacity of the EV may remain unused in this technique. So, further studies are suggested to find out the optimal value for the bandwidth of the CBESS power smoothing filter. Besides, if the EV companies, provides the specifications of the EV power management system, in a way that this information is easily accessible for the EV charger or the MG controller, it can significantly facilitate the implementation of this work and enhance the efficiency of the proposed EV charging method.

VII. CONCLUSION

This paper proposes a method for utilizing the internal SC of EVs with battery-SC HESS technologies to absorb the instantaneous power variations in an islanded building-scale DC MG. The primary goal of this method is to increase the lifetime of the MG's CBESS and improve the performance of the MG voltage control system. Wherefore, an adaptive FB current allocation system is designed which assigns the high-frequency current variations to the internal SC of the EV and the low-frequency current variations to the CBESS without impacting the charge current of the EV's BESS. So, the output current/power of the MG's CBESS is smoothed while the charging profile of the EV's BESS is not affected. In other words, using the proposed EV charging method, the lifetime of the MG's CBESS can be improved without degrading the internal BESS of the EV. In addition, a small-signal stability analysis is performed to assess the impact of the proposed EV charging method on the voltage stability of an islanded building-scale DC MGs. The stability analysis indicates that the stability margin of the DC MG increases during the charging process of the EV with the proposed method enabling the PI voltage controller to operate with higher gains. Hence, the MG voltage controller can provide faster responses to load variations, thereby reducing the transient voltage deviations

during sudden load changes. Then, the performance of the proposed approach is validated using MATLAB/Simulink as well as a HIL testbed that employs a real-time OPAL-RT simulator, and a Raspberry Pi microprocessor. The simulation results show that the CBESS has 86% fewer power variations using the proposed approach. Besides, the HIL testing results shows that the transient voltage quality of the system is improved by reducing the amplitude of the voltage deviations and shortening the settling time of the DC bus voltage variations in a specific load change scenario.

REFERENCES

[1] Y. Wang, A. O. Rousis, and G. Strbac, "On microgrids and resilience: A comprehensive review on modeling and operational strategies," *Renew. Sustain. Energy Rev.*, vol. 134, p. 110313, Dec. 2020.

[2] C. Zhang, X. Wang, P. Lin, P. X. Liu, Y. Yan, and J. Yang, "Finite-time feedforward decoupling and precise decentralized control for DC microgrids towards large-signal stability," *IEEE Trans. Smart Grid*, vol. 11, no. 1, pp. 391–402, Jan. 2020.

[3] K. K. Nandini, N. S. Jayalakshmi, and V. K. Jadoun, "An overview of DC Microgrid with DC distribution system for DC loads," *Mater. Today Proc.*, vol. 51, pp. 635–639, Jan. 2022.

[4] J. Wang, C. Dong, C. Jin, P. Lin, and P. Wang, "Distributed uniform control for parallel bidirectional interlinking converters for resilient operation of hybrid AC/DC microgrid," *IEEE Trans. Sustain. Energy*, vol. 13, no. 1, pp. 3–13, Jan. 2022.

[5] D. Dong, F. Luo, X. Zhang, D. Boroyevich, and P. Mattavelli, "Grid-interface bidirectional converter for residential DC distribution systems - Part 2: AC and DC interface design with passive components minimization," *IEEE Trans. Power Electron.*, vol. 28, no. 4, pp. 1667–1679, Apr. 2013.

[6] A. Cano, P. Arévalo, D. Benavides, and F. Jurado, "Comparative analysis of HESS (battery/supercapacitor) for power smoothing of PV/HKT, simulation and experimental analysis," *J. Power Sources*, vol. 549, p. 232137, Nov. 2022.

[7] K. Uddin, A. D. Moore, A. Barai, and J. Marco, "The effects of high frequency current ripple on electric vehicle battery performance," *Appl. Energy*, vol. 178, pp. 142–154, Sep. 2016.

[8] S. Gunther, L. Weber, A. L. Bensmann, and R. Hanke-Rauschenbach, "Structured analysis and review of filter-based control strategies for hybrid energy storage systems," *IEEE Access*, vol. 10, pp. 126269-126284, Dec. 2022.

[9] P. K. Singha Roy, H. B. Karayaka, J. He and Y. -H. Yu, "Economic comparison between battery and supercapacitor for hourly dispatching wave energy converter power," *2020 52nd North American Power Symposium (NAPS)*, Tempe, AZ, USA, Apr. 2021, pp. 1-6.

[10] C. Wang, R. Xiong, H. He, Y. Zhang, and W. Shen, "Comparison of decomposition levels for wavelet transform based energy management in a plug-in hybrid electric vehicle," *J. Clean. Prod.*, vol. 210, pp. 1085–1097, Feb. 2019.

[11] S. A. Ghorashi Khalil Abadi and A. Bidram, "A distributed rule-based power management strategy in a photovoltaic/hybrid energy storage based on an active compensation filtering technique," *IET Renew. Power Gener.*, vol. 15, no. 15, pp. 3688-3703, Nov. 2021.

[12] K. J. Lim, L. W. Chong, S. Morris, B. H. Lim, M. Fahmi, and C. Palanichamy, "Battery lifetime and life cycle cost analysis of battery-supercapacitor hybrid energy storage system for standalone power system," in *2022 IEEE 5th International Symposium in Robotics and Manufacturing Automation* , Oct. 2022, pp. 1–6.

[13] H. M. Mehdi, M. K. Azeem, and I. Ahmad, "Artificial intelligence based nonlinear control of hybrid DC microgrid for dynamic stability and bidirectional power flow," *J. Energy Storage*, vol. 58, p. 106333, Feb. 2023.

[14] S. Kotra and M. K. Mishra, "Design and stability analysis of DC microgrid with hybrid energy storage system," *IEEE Trans. Sustain. Energy*, vol. 10, no. 3, pp. 1603–1612, Jan. 2019.

[15] S. A. Ghorashi Khalil Abadi, S. I. Habibi, T. Khalili, and A. Bidram, "A model predictive control strategy for performance improvement of hybrid energy storage systems in DC microgrids," *IEEE Access*, vol. 10, pp. 25400–25421, Feb. 2022.

[16] M. Zhang, Q. Xu, C. Zhang, L. Nordstrom, and F. Blaabjerg, "Decentralized coordination and stabilization of hybrid energy storage systems in DC microgrids," *IEEE Trans. Smart Grid*, vol. 13, no. 3, pp. 1751–1761, May 2022,

[17] S. Singh, A. R. Gautam, and D. Fulwani, "Constant power loads and their effects in DC distributed power systems: A review," *Renew. Sustain. Energy Rev.*, vol. 72, pp. 407–421, 2017, May. 2017.

[18] S. A. Ghorashi Khalil Abadi, T. Khalili, S. I. Habibi, A. Bidram, and J. M. Guerrero, "Adaptive control and management of multiple nano-grids in an islanded dc microgrid system," *IET Gener. Transm. Distrib.*, Jul. 2022.

[19] A. Kwasinski and C. N. Onwuchekwa, "Dynamic behavior and stabilization of DC microgrids with instantaneous constant-power loads," *IEEE Trans. Power Electron.*, vol. 26, no. 3, pp. 822–834, Mar. 2011.

[20] M. WU and D. D. C. LU, "Active stabilization methods of electric power systems with constant power loads: a review," *J. Mod. Power Syst. Clean Energy*, vol. 2, no. 3, pp. 233–243, Jan. 2014.

[21] M. A. Hassan *et al.*, "DC shipboard microgrids with constant power loads: A review of advanced nonlinear control strategies and stabilization techniques," *IEEE Trans. Smart Grid*, Sep. 2022.

[22] R. Kumar and C. N. Bhende, "A virtual adaptive RC damper control method to suppress voltage oscillation in DC microgrid," *Int. J. Electr. Power Energy Syst.*, vol. 146, p. 108795, Mar. 2023.

[23] Z. Karami, Q. Shafiee, S. Sahoo, M. Yaribeygi, H. Bevrani, and T. Dragicevic, "Hybrid model predictive control of DC-DC boost converters with constant power load," *IEEE Trans. Energy Convers.*, vol. 36, no. 2, pp. 1347–1356, Jun. 2021.

[24] J. A. Sanguesa, V. Torres-Sanz, P. Garrido, F. J. Martinez, and J. M. Marquez-Barja, "A review on electric vehicles: Technologies and challenges," *Smart Cities*, vol. 4, no. 1, pp. 372–404, Mar. 2021.

[25] D. D. Tran, M. Vafaeipour, M. El Baghdadi, R. Barrero, J. Van Mierlo, and O. Hegazy, "Thorough state-of-the-art analysis of electric and hybrid vehicle powertrains: Topologies and integrated energy management strategies," *Renew. Sustain. Energy Rev.*, vol. 119, p. 109596, Mar. 2020

[26] Q. Zhang and G. Li, "Experimental study on a semi-active battery-supercapacitor hybrid energy storage system for electric vehicle application," *IEEE Trans. Power Electron.*, vol. 35, no. 1, pp. 1014–1021, Jan. 2020.

[27] F. Gonzalez Venegas, M. Petit, and Y. Perez, "Active integration of electric vehicles into distribution grids: Barriers and frameworks for flexibility services," *Renew. Sustain. Energy Rev.*, vol. 145, p. 111060, Jul. 2021.

[28] K. M. Tan, V. K. Ramachandaramurthy, and J. Y. Yong, "Integration of electric vehicles in smart grid: A review on vehicle to grid technologies and optimization techniques," *Renew. Sustain. Energy Rev.*, vol. 53, pp. 720–732, Jan. 2016.

[29] M. Brenna, F. Foiadelli, C. Leone, and M. Longo, "Electric vehicles charging technology review and optimal size estimation," *J. Electr. Eng. Technol.*, vol. 15, no. 6, pp. 2539–2552, Nov. 2020.

[30] S. H. Leung and C. F. So, "Gradient-based variable forgetting factor RLS algorithm in time-varying environments," *IEEE Trans. Signal Process.*, vol. 53, no. 8, pp. 3141–3150, Aug. 2005.

[31] K. Gu, J. Chen, and V. Kharitonov, *Stability of time-delay systems*. 2003.

Seyyed Ali Ghorashi Khalil Abadi (S'20) received the B.S. degree from Ferdowsi University of Mashhad, Mashhad, Iran in 2014 and the M.S degree from Amirkabir University of Technology, Tehran, Iran in 2017 both in electrical engineering-control. He is currently a Ph.D. student in the University of New Mexico, Albuquerque, USA. His main research interests include control and management of DC microgrids, model predictive control, supervisory control and hybrid energy storage systems. He has received Zacanda graduate fellowship award by the Office of Vice President for Research (OVPR), University of New Mexico in 2022, and Talented Student award by Amirkabir University of Technology in 2017.

Jeewon Choi (S'20) received her B.S. degree in mechanical and automotive engineering from Keimyung University, Daegu, South Korea, in 2015, M.S. and Ph.D. in mechanical engineering from the University of New Mexico, Albuquerque, NM, USA, in 2018 and 2022. Her research interests include smart grid, microgrid, and cyber-physical system modeling and simulation.

Ali Bidram (S'12–M'17) received the B.Sc. and M.Sc. degrees from the Isfahan University of Technology, Iran, in 2008 and 2010, respectively, and the Ph.D. degree from The University of Texas at Arlington, USA, in 2014. Before joining The University of New Mexico, he worked with Quanta Technology, LLC, and was involved in a wide range of projects in electric power industry. He is currently an Assistant Professor with the Electrical and Computer Engineering Department, The University of New Mexico, Albuquerque, NM, USA. Such research efforts are culminated in a book, several journal articles in top publication venues and papers in peer-reviewed conference proceedings, and technical reports.

His area of interest includes control and coordination of energy assets in power electronics-intensive energy distribution grids. He is an Associate Editor for the IEEE Transaction on Industry Applications. His area of expertise lies within control and coordination of energy assets in power electronics-intensive energy distribution grids. Such research efforts are culminated in a book, several journal papers in top publication venues and articles in peer-reviewed conference proceedings, and technical reports. He has received IEEE Albuquerque section outstanding engineering educator award, New Mexico EPSCoR mentorship award, University of Texas at Arlington N. M. Stelmakh outstanding student research award, Quanta Technology Shooting Star award, IEEE Kansas Power and Energy Conference best paper award, and cover article of December 2014 in IEEE Control Systems.